





60 GHz Bandwidth Directly Modulated Membrane III-V Lasers on SiO₂/Si

Nikolaos-Panteleimon Diamantopoulos , *Member, IEEE*, Takuro Fujii , *Member, IEEE*, Suguru Yamaoka, Hidetaka Nishi, *Member, IEEE*, Koji Takeda , *Senior Member, IEEE*, Tai Tsuchizawa, Toru Segawa, *Member, IEEE*, Takaaki Kakitsuka , *Member, IEEE*, and Shinji Matsuo, *Fellow, IEEE*

(Top-Scored Paper)

Abstract—Increasing demand for higher data rates in data centers and high-performance computing systems require optical interconnects that support more than 100 Gbps-per-lane. Meanwhile, as optics are packed ever closer to Ethernet switches and electronic processors, both operating temperatures and power consumptions increase, resulting in increasing operational and environmental costs. In this work we present our recent results on a two-channel energy-efficient directly modulated membrane laser array on SiO₂/Si with ~60-GHz 3-dB bandwidth, that can support both 100 Gbps-per-lane modulations as well as very small form-factors and power consumptions. The extension to 60 GHz bandwidths denotes a ~26.3% increase compared to previous works, and it was achieved based on an optimized distributed-reflector laser design for maximizing the photon-photon resonance effect. Based on the fabricated two-channel DML array, 200 Gbps (2×112-Gbps NRZ) with laser operating energy-per-bit cost of less than 0.3 pJ/bit over 2-km transmissions, and the feasibility of 400 Gbps (2×200-Gbps PAM-4) transmissions are demonstrated. Finally, the temperature dependence of the PPR effect and its impact on the E-O response have been studied both experimentally and with numerical simulations for temperatures up to 75 °C for the first time.

Index Terms—Directly modulated lasers, III-V/Si technology, integrated photonics.

I. INTRODUCTION

THE increasing traffic growth in data center networks due to the rise of cloud-computing services [1] have pushed recent Ethernet standardizations to rely on optical interconnects with data rates of 200 and 400 Gbps [2]. Following this

Manuscript received November 15, 2021; revised February 15, 2022; accepted February 18, 2022. Date of publication February 23, 2022; date of current version May 25, 2022. (Corresponding author: Nikolaos-Panteleimon Diamantopoulos.)

Nikolaos-Panteleimon Diamantopoulos, Takuro Fujii, Suguru Yamaoka, Hidetaka Nishi, Koji Takeda, Tai Tsuchizawa, Toru Segawa, and Shinji Matsuo are with NTT Device Technology Labs, Nippon Telegraph and Telephone Corporation, Atsugi, Kanagawa 243-0198, Japan (e-mail: np.diamantopoulos.pb@hco.ntt.co.jp; takuro.fujii.uc@hco.ntt.co.jp; suguru.yamaoka.hm@hco.ntt.co.jp; hidetaka.nishi.sf@hco.ntt.co.jp; koji.takeda.vk@hco.ntt.co.jp; tai.tsuchizawa.ya@hco.ntt.co.jp; toru.segawa.re@hco.ntt.co.jp; shinji.matsuo.vm@hco.ntt.co.jp).

Takaaki Kakitsuka is with NTT Device Technology Labs, Nippon Telegraph and Telephone Corporation, Atsugi, Kanagawa 243-0198, Japan, and also with the Graduate School of Information, Production and Systems, Waseda University, Kitakyushu, Fukuoka 808-0135, Japan (e-mail: t.kakitsuka@waseda.jp).

Color versions of one or more figures in this article are available at <https://doi.org/10.1109/JLT.2022.3153648>.

Digital Object Identifier 10.1109/JLT.2022.3153648

trend, near-future targets of 800 Gbps and beyond 1 Tbps have been set, assuming optical interconnects that utilize more than 100 Gbps-per-lane [3]. Meanwhile, on-board and co-packaged optics (OBO/CPO) are increasingly gaining traction on bringing small form-factor optical transceivers (TRx) closer to Ethernet switches and electronic processing units for data center and high-performance computing systems [4]. However, as data rates rise and more components are packed closer together, operating temperatures and power consumptions increase as a result. This further leads to increasing operational costs, as well as an increasingly worrisome environmental impact [5].

One of the most promising components for reducing the power consumption and footprint of optical TRxs, is the low-operating-power directly modulated laser (DML) [6]. Membrane III-V DMLs [6]–[8], in particular, can achieve both a large bandwidth as well as a very low power consumption, owing to their high optical confinement factor. Arrays of energy-efficient membrane III-V DMLs on SiO₂/Si have been demonstrated for 200/400 Gbps systems utilizing wavelength- or space-division multiplexing (WDM/SDM) [9]–[11]; with the fabrication on Si being a critical step towards achieving low-cost production via large Si wafers.

In conventional DMLs, however, there exists an inherent tradeoff between modulation bandwidth and power consumption due to the dependence of the carrier-photon resonance (CPR) dynamics on the operating bias current [8]. Recent longitudinal laser designs have addressed this limitation by carefully designing optical cavities that can enable the photon-photon resonance (PPR) effect [8], [12]–[18] – i.e., the enhancement of the electro-optic (E-O) response via the presence of a secondary longitudinal mode close in frequency to the main lasing mode. Based on the PPR effect, InP lasers with more than 65 GHz 3-dB bandwidths have been realized [15], with a record of 108 GHz 3-dB bandwidth been achieved by a membrane III-V laser on a high-thermal-conductivity SiC substrate [16]. Also, by combining PPR-based DMLs with advanced digital signal processing (DSP) and probabilistically-shaped modulation formats, single-lane gross rates of more than 400 Gbps have been demonstrated [19], [20].

In our previous work on membrane III-V on SiO₂/Si DMLs [8] we were able to extend the DML bandwidth from ~20 GHz (without PPR) to ~47.5 GHz (with PPR) while keeping the

same power consumption, by using a distributed reflector (DR) laser structure which relied on a distributed Bragg reflector (DBR) for enabling the PPR effect. Based on it, we could demonstrate four-level pulse-amplitude modulation (PAM-4) of up to 120 Gbps by using low-complexity nonlinear equalization [8], [21]. The reliance, however, on high-order modulation formats and nonlinear equalization, could increase significantly the overall power consumption of the system due to the additional requirements for linear drivers and RF amplifiers, and increased DSP complexity [21]. For a more energy-efficient system, therefore, high-symbol-rate non-return-to-zero (NRZ) modulation via high-bandwidth, yet energy-efficient, DMLs is a more preferable solution. Moreover, even though we have previously demonstrated more than 100-Gbps NRZ short-reach transmission with our PPR-based membrane DMLs on SiC [18], achieving a likewise performance on membrane DMLs fabricated on SiO₂/Si is of both high industrial and scientific interest.

In this extended paper we expand on our recently-presented work [22], in which we have achieved a further 3-dB bandwidth extension of up to 60 GHz at O-band (i.e., $\sim 26.3\%$ increase compared to [8]) on a two-channel membrane DML array on SiO₂/Si by optimizing our PPR-enabling membrane DR structure. Based on this 60-GHz two-channel DML array we could demonstrate 2×112 -Gbps NRZ signals with < 0.3 pJ/bit operating energy without any complicated DSP, as well as the feasibility of 2×200 -Gbps PAM-4 signals. Moreover, in this paper we further discuss the performance of our DMLs and the PPR effect at higher operating temperatures up to 75 °C, which is of high interest for commercial applications. In particular, experimentally-obtained E-O responses with PPR enhancements at high temperatures are presented and evaluated with numerical simulations.

The paper is organized as follows. Following the introduction in Section I, the optimized PPR laser design and two-channel array fabrication are presented in Section II. Following that, the 2×112 -Gbps NRZ and 2×200 -Gbps PAM-4 demonstrations are presented in Section III. At last, the new results and discussions on high temperature operation are included in Section IV, following a conclusion in Section V.

II. DESIGN AND FABRICATION

A. PPR Optimization

In our conventional membrane lasers [6], [7], single-longitudinal-mode lasing is achieved by a DR laser structure composed of a zero-shifted distributed-feedback (DFB) section based on multiple-quantum wells (MQWs) and a detuned InP-based rear DBR section (DBR-r). In this DR laser structure, DBR-r is used to filter out one of the two main longitudinal DFB modes. Such a longitudinal laser structure reduces the impact of the spatial hole-burning effect in comparison to standard $\lambda/4$ -shifted DFB lasers. One way to introduce the PPR effect in this structure is by including an additional InP-based front DBR section (DBR-f) as shown schematically in Fig. 1. In this case, DBR-f is designed to have a Bragg wavelength similar to that of the DFB section as discusses in details in Ref. [8]. Moreover, by operating on the long-wavelength side-lobe of DBR-f, the

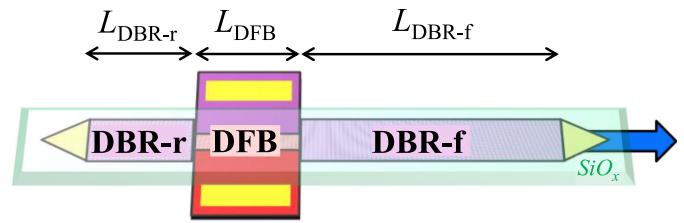


Fig. 1. Longitudinal laser design for photon-photon resonance.

relaxation oscillation frequency f_R can be enhanced due to the detuned-loading effect [8], [16], [23]. In our previous work [8], the lengths of the DFB, DBR-r, and DBR-f sections were $L_{DFB} = 100 \mu\text{m}$, $L_{DBR-r} = 80 \mu\text{m}$, and $L_{DBR-f} = 200 \mu\text{m}$, respectively. Uniform surface gratings on InP were assumed for all sections, with a coupling coefficient κ of around 524 cm^{-1} for the DFB section and around 400 cm^{-1} for the DBR sections. Based on this design, a f_R of more than 15 GHz and a PPR frequency f_{PPR} of around 40 GHz were achieved, resulting in a maximum 3-dB bandwidth of around 47.5 GHz at 25 °C [8].

One key parameter for maximizing the 3-dB bandwidth in PPR-enabled DMLs is the frequency separation between the PPR and CPR effects, namely $\Delta f_{PPR-CPR} = f_{PPR} - f_R$. On one hand, a large $\Delta f_{PPR-CPR}$ results in a significant “dip” in the E-O response which is below the desired -3 dB limit. On the other hand, a very small $\Delta f_{PPR-CPR}$ doesn’t utilize the full potential of the PPR effect, hindering thus the maximization potential of the E-O response bandwidth. In either case an undesired non-flat or “bumpy” E-O response is typically observed [15], which is not suitable for popular single-carrier modulation formats such as PAM-4 and NRZ. Since in our previous work [8], $\Delta f_{PPR-CPR}$ appeared to be below its optimum value, in this improved design we aimed at increasing f_{PPR} from ~ 40 GHz previously, to ~ 50 GHz. This yields an optimized $\Delta f_{PPR-CPR}$ separation of ~ 30 GHz and an extended 3-dB bandwidth of 60 GHz.

This was achieved by considering how f_{PPR} is affected by the parameters defining the DFB section of our DR laser structure. Since f_{PPR} is proportional to the wavelength separation between the main longitudinal lasing mode and its nearest side-mode [8], and by assuming a fixed κ and effective index n_{eff} for all sections, this can be achieved by decreasing the DFB length. Such a relationship can be readily understood by observing the transmittance spectrum of the DFB section shown in Fig. 2(a). As it can be seen from this figure, the separation between the dominant DFB mode(s) and its (their) nearest side-mode(s) decreases by increasing the DFB length L_{DFB} . Therefore, an increased $\Delta f_{PPR-CPR}$ can be achieved by reducing L_{DFB} . This can be further confirmed by the modal analysis (see [8], [24]) of our DR structure shown in Fig. 2(b). Here the horizontal axis defines the wavelength detuning from the DFB’s Bragg wavelength and the vertical axis the mode damping (note: the mode threshold is reached for zero damping and a mode is lasing for negative damping values). Based on this modal analysis, a relationship between f_{PPR} and L_{DFB} can be derived as shown in Fig. 2(c). Considering, therefore, our $\Delta f_{PPR-CPR}$ target of ~ 30 GHz (i.e., f_{PPR} of ~ 50 GHz), the

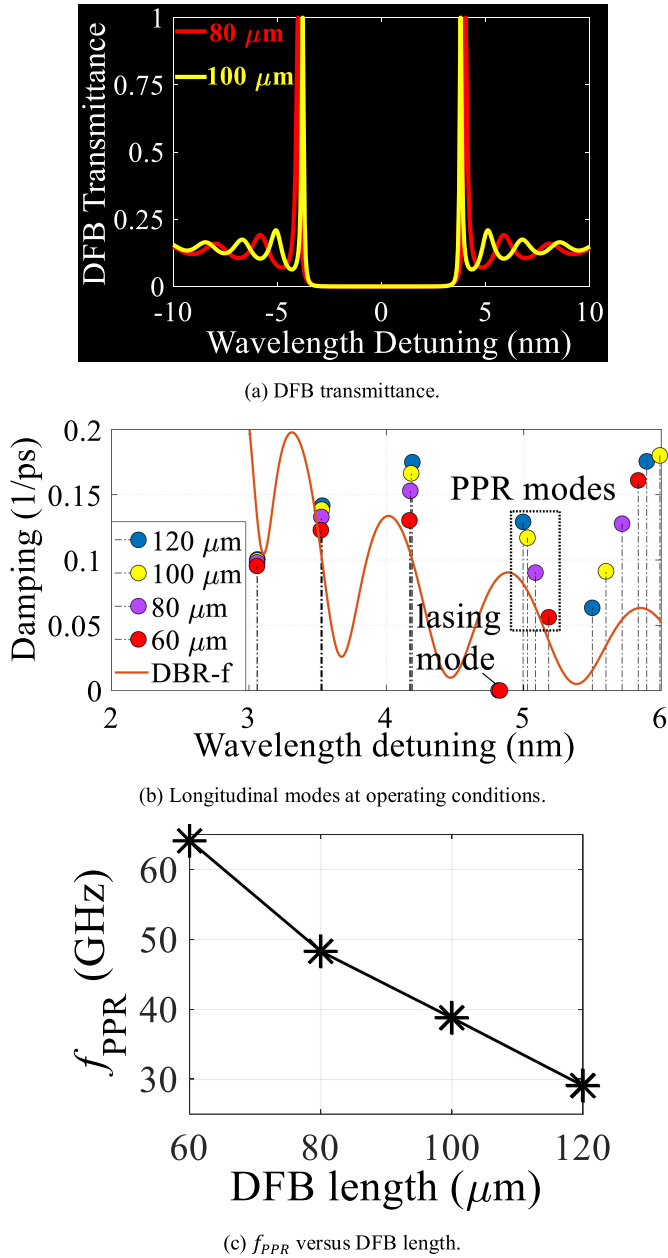


Fig. 2. Optimization of photon-photon resonance condition.

optimized DFB length is $L_{DFB} = 80 \mu\text{m}$ (instead of $100 \mu\text{m}$ used previously).

B. Two-Channel DML Array

The cross-sectional schematic of our membrane DR laser on SiO₂/Si is depicted in Fig. 3(a). To achieve both high optical and high carrier confinement we utilize a buried heterostructure with a lateral *p-n* junction, with total III-V thickness of less than 350 nm [6]–[8]. For O-band operation we use InGaAlAs-based MQWs with an active core width of 600 nm and total MQW thickness of around 103 nm. The confinement factor for this structure was estimated to be around 14%. Low-loss coupling to high-numerical aperture fibers is achieved via a spot-size converter composed of an InP taper and a $3 \times 3 \mu\text{m}^2$ SiO_x waveguide

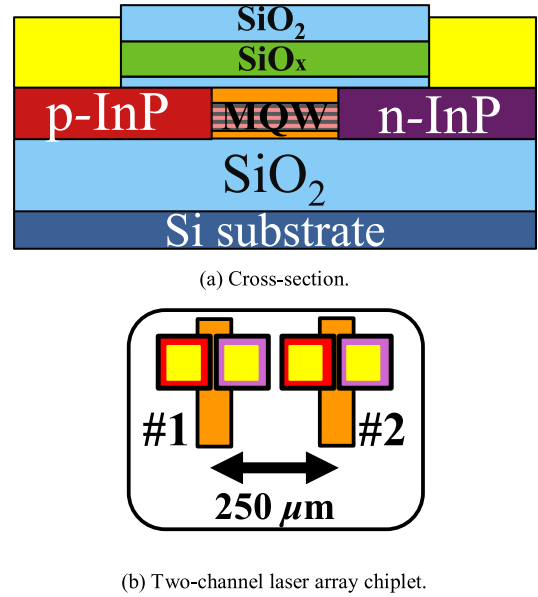


Fig. 3. Fabricated laser array structure.

with SiO₂ cladding [7]. The width of the passive InP waveguides used for the DBRs was $1.5 \mu\text{m}$. As shown by Fig. 3(b) a two-channel laser array was fabricated with a laser pitch of $250 \mu\text{m}$, in order to avoid electrical and thermal crosstalk.

The static, fiber-coupled L-I-V characteristics of the two-channel array at a stage-controlled room temperature of 25°C are shown in Fig. 4(a). Super-linear L-I curves are observed for both devices between kinks defined by mode hoppings. This is a typical behavior for DBR-based PPR lasers [8], [16], while the mode hoppings correspond to different side-lobes/modes of DBR-f [8]. The fiber-coupled output power for both DMLs were between 0 to 1 dBm and the voltages bias were below 2 V for bias currents up to 15 mA. These output power levels are similar to previously demonstrated membrane DR lasers on SiO₂/Si that didn't include the DBR-f section [7], [11]. The static spectra for both DMLs are depicted by solid lines in Fig. 4(b) at operating bias currents. In both DMLs the presence of a PPR side-mode is confirmed, with lasing wavelengths of around 1294.3 nm for CH#1 and 1295.1 nm for CH#2. The small wavelength variation is attributed to a minor Bragg wavelength change due to fabrication.

At last, the experimental E-O responses for the two channels are shown in Fig. 4(c), together with an experimental E-O response for the $100\text{-}\mu\text{m}$ -long DFB-section DR laser of Ref. [8], at the same operating bias current as CH#2 as a reference. Apart from the DFB lengths, all structures and fabrications procedures were similar for these lasers. As it can be seen, the 3-dB bandwidths of both lasers in the two-channel array were around 60 GHz, which denotes a $\sim 26.3\%$ increase compared to the $100\text{-}\mu\text{m}$ -long DFB case. The small Bragg wavelength deviation between CH#1 and CH#2 resulted in a smaller bias current for CH#1 for achieving the 60-GHz bandwidth when compared to CH#2. Note that, a further reduction of L_{DFB} would have increased $\Delta f_{PPR-CPR}$ according to Fig. 2(c). This would have resulted in a dip between f_R and f_{PPR} that would have hindered the flatness and 3-dB bandwidth of the E-O response.

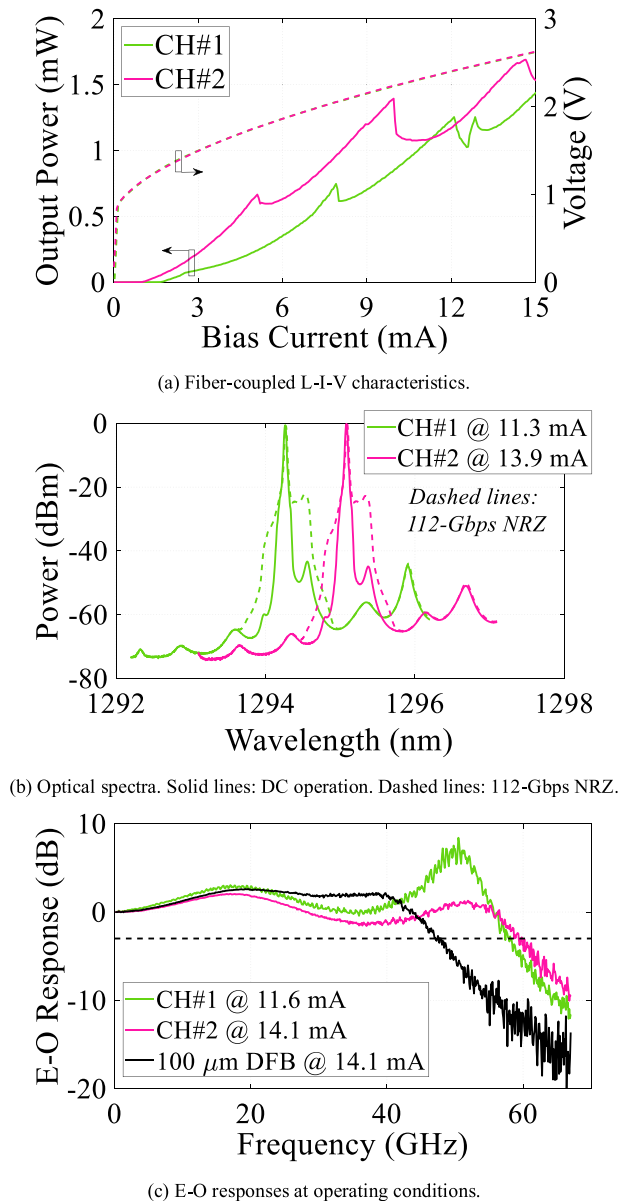


Fig. 4. Characterization of fabricated two-laser array.

III. EXPERIMENTAL DEMONSTRATION

For the experimental demonstration of the two-channel DML array we prepared a typical short-reach intensity-modulated directly-detected setup [8], [11] based on 112 Gbps NRZ and 100 GBaud PAM-4 (200 Gbps) signals. The NRZ and PAM-4 signals were generated by a Keysight M8194A arbitrary waveform generator (AWG) at 128 GSa/s, using a root-raised cosine filter with 10% rolloff factor. The analogue 3-dB bandwidth of the AWG was 60 GHz. For the 112 Gbps NRZ case, the signals were generated with a peak-to-peak voltage of 120 mV and 140 mV for CH#1 and CH#2, respectively. All signals were amplified by an RF driver with 22-dB gain and 60-GHz 3-dB bandwidth. The DML array was driven by a bias-T with 65-GHz 3-dB bandwidth and an RF probe with 65-GHz 3-dB bandwidth. The DML array chip was operated at a stage-controlled room-temperature of 25 °C. By using a multi-channel RF probe

as in Ref. [11] prior to the measurements, it was confirmed that no observable electrical/RF or optical crosstalk existed between the two channels. Therefore, subsequent measurements were performed on a channel-by-channel basis.

For the 112 Gbps NRZ case, the bias currents and voltages were 11.3 mA and 2.347 V for CH#1 and 13.9 mA and 2.517 V for CH#2. Therefore, the operating energies were around 26.5 mW and around 35.0 mW for CH#1 and CH#2, respectively. The modulated optical spectra for both channels are shown in Fig. 4(b). As it can be seen from this figure, the PPR side-mode clearly amplifies the modulated signal at high frequencies, as expected from the obtained E-O response measurements.

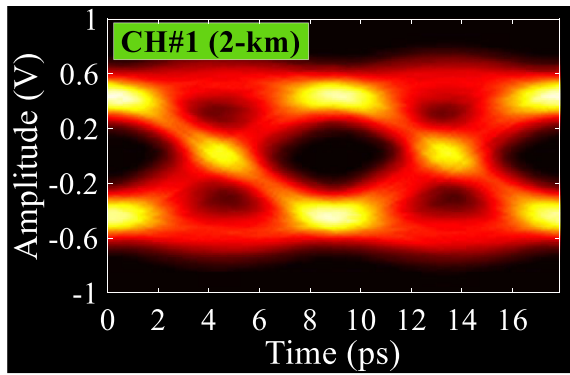
Bit-error rates (BERs) were measured at an optical back-to-back (BTB) configuration or after 2-km of standard single-mode fiber (SSMF) transmissions, by varying the received optical power (ROP) using an optical variable attenuator. The photodiode used for detection was an in-house uni-travelling-carrier photodetector (UTC-PD) with a 3-dB bandwidth of more than 67 GHz and a responsivity of around 0.23 A/W. Due to the lack of a trans-impedance amplifier, a commercial RF amplifier with 18-dB gain and 67-GHz 3-dB bandwidth was used after the UTC-PD for signal amplification. Finally, a real-time digital sampling oscilloscope (DSO) was for analogue-to-digital conversion at 160 GSa/s. The analogue bandwidth of the DSO was 67 GHz. Regarding (offline) digital equalization, for the 112-Gbps NRZ signals an 11-tap linear pre-emphasis filter was used at the transmitter side in order to mitigate RF impairments due to RF probe, RF cables, etc., and a 5-tap decision-feedback equalizer was used at the receiver side. For the 200-Gbps PAM-4 measurements, a receiver-side pruned Volterra filter was used [21] with 101 linear taps, 51 nonlinear taps, and a pruning factor of 10. The resulting equalized eye diagrams for 112-Gbps signals after 2-km SSMF transmissions for both CH#1 and CH#2, and 200-Gbps PAM-4 signals at BTB for CH#2 are shown in Fig. 5. The performance of 200-Gbps PAM-4 signals for CH#1 was similar to or slightly worse than CH#2.

The resulting BERs versus ROPs are summarized in Fig. 6. For all 112-Gbps NRZ transmissions, the 200/400-Gbps Ethernet standard of KP4 forward-error correction (KP4-FEC) threshold [2] has been reached. Considering the operating energies of 26.5 mW and 35.0 mW for CH#1 and CH#2, respectively, the resulting energy-per-bit costs were 0.24 pJ/bit for CH#1 and 0.31 pJ/bit for CH#2. Furthermore, if we take into consideration the 5.8% overhead for KP4-FEC [2], the aggregate net rate of 211.72 Gbps was achieved with an energy-per-bit cost of $(0.24 + 0.31) \text{ mW} / 211.72 \text{ Gbps} \approx 0.29 \text{ pJ/bit}$.

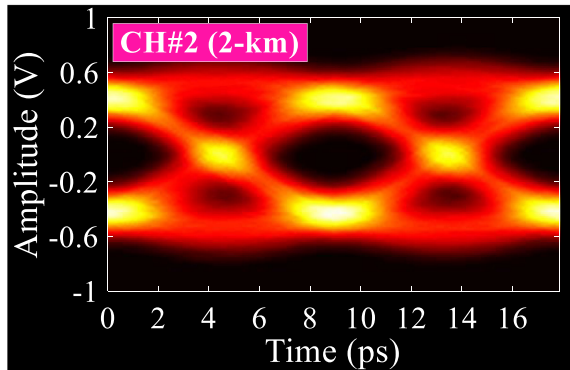
Finally, regarding the 200-Gbps PAM-4 signal modulations, the resulting BERs were around $1.58\text{E-}2$ and $7.25\text{E-}3$ for CH#1 and CH#2, respectively, at BTB. Even though these BERs cannot reach the KP4-FEC threshold, they can still be reached by a higher-overhead hard-decision FEC (HD-FEC) [25] at the expense of higher power consumption and latency.

IV. DISCUSSIONS ON HIGH-TEMPERATURE OPERATION

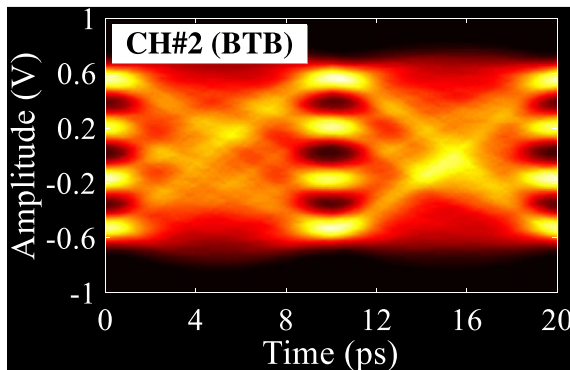
As discussed in Section I, it is of great important to evaluate the performance of our DML array and PPR effect at higher



(a) CH#1: 112 Gbps NRZ after 2-km SSMF.



(b) CH#2: 112 Gbps NRZ after 2-km SSMF.



(c) CH#2: 200-Gbps PAM-4 at back-to-back (BTB).

Fig. 5. Obtained eye diagrams after receiver equalization at maximum ROPs.

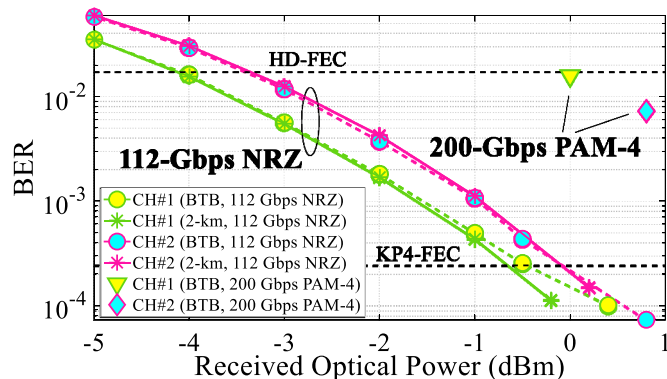
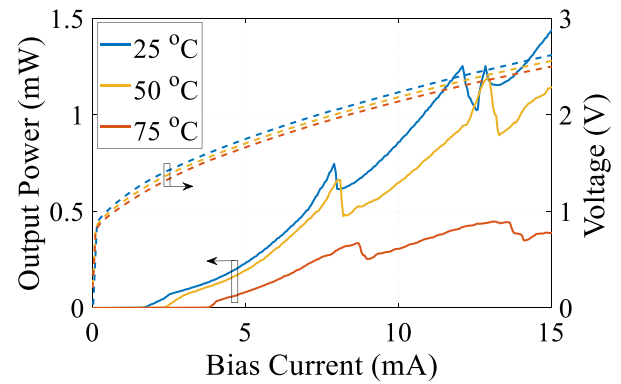
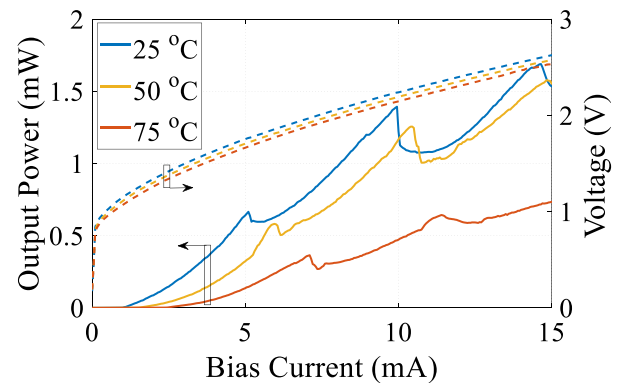


Fig. 6. Bit-error rate (BER) versus received optical power (ROP).



(a) CH #1.



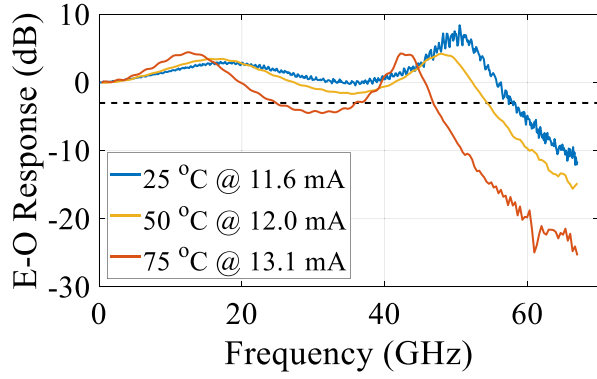
(b) CH #2.

Fig. 7. Temperature dependence of L-I-V characteristics.

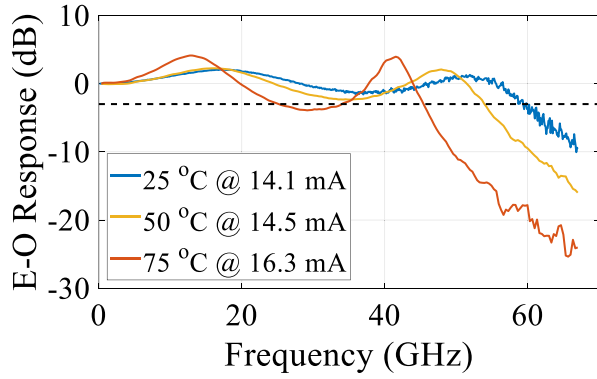
temperatures occurring in realistic application scenarios. In regards to the PPR effect in particular, there are currently very limited or no available studies regarding its temperature dependence. In a previous demonstration, we have demonstrated PPR-enhanced E-O responses and 120-Gbps PAM-4 modulations up to 50 °C [8]. However, even though a reduction of the f_{PPR} at 50 °C was observed, no physical justification of such a behavior was provided at the time. In this section, we experimentally study the PPR-enhancement effect at temperatures up to 75 °C based on our two-channel DML array. In addition, for the first time numerical simulations are carried out in order to provide a concrete understanding on the physics behind its temperature dependence.

The experimentally obtained L-I-V and E-O responses for our two-channel DML array for up to 75 °C are shown in Fig. 7 and Fig. 8, respectively. As expected, the output power is reduced at higher temperatures due to reduction of the gain at high temperatures. Also, as is well known, for a similar reason the f_R is also reduced at higher temperatures. Nevertheless, the extended 3-dB bandwidth at 75 °C remains above 45 GHz, which could support 100-Gbps-class signals based on PAM-4 modulation, based on our previous demonstrations (Ref. [8]).

Considering the temperature dependence on the PPR effect we can make a few observations based on Figs. 7 and 8. Firstly, L-I maintains the super-linear behavior and mode-hoppings. This is because the effective indexes n_{eff} of the DFB and DBR



(a) CH #1.



(b) CH #2.

Fig. 8. Temperature dependence of E-O response.

sections are both affected by the temperature rise. Therefore, a PPR relationship based on DBR-f and DFB is maintained. However, mode-hoppings occur for higher bias currents at higher temperatures. This is because the dependence of the n_{eff} on the temperature is slightly different for the MQW core (DFB section) and InP waveguide (DBR sections). Since the PPR effect is mainly observed at bias currents in the vicinity the mode-hopping regions, it is also expected that the maximization of the PPR-enhancement effect on the E-O response will also occur at slightly higher bias currents. This explains why, even though the optimum operating bias current for maximizing the modulation bandwidth at 25 °C is 14.1 mA, the optimum bias currents for 50 °C and 75 °C are 14.5 mA and 16.3 mA, respectively. However, since the bias current deviation is only within ± 1.1 mA simple control electronics, typically found in DML transmitters, can be utilized as real-time adjustment mechanisms for the bias currents, without any need for costly and extra power-consuming heaters.

Another very significant observation is the fact that f_{PPR} decreases at higher temperatures. Actually, this is rather beneficial because f_R is also reduced at higher temperatures. Therefore, a good $\Delta f_{PPR-CPR}$ relationship can be maintained even as the temperature deviates. However, in order to clarify the physical reason behind this reduction of f_{PPR} at higher temperatures, we need to consider the temperature dependence of both the gain and n_{eff} via numerical simulations. Here, the dynamic

travelling-wave model coupled to a rate equation for carrier density [8], [26] was used for the numerical analysis of the longitudinal DR structure of our DMLs.

Firstly, we derived logarithmic relationships for the gain in our DMLs [11] for different operating temperatures, based on experimental observations on the two-channel DML chip using the detected values for f_R and threshold currents I_{th} among others. The resulting gain relationships are plotted in Fig. 9(a). Then, by simulating the E-O responses based on either only the temperature dependence of n_{eff} (Fig. 9(b)) or only the temperature dependence of gain (Fig. 9(c)), we could separate the two effects and their contribution on f_{PPR} . Regarding the modelling of the temperature dependence of n_{eff} , the following linear relationships were used:

$$n_{eff,DBR}(T) = n_{eff,DBR,0} + \Delta T \frac{\partial n_{eff,DBR}(T)}{\partial T}, \quad (1)$$

$$n_{eff,DBR,0} \equiv n_{eff,DBR}(T = 25^\circ\text{C}), \quad (2)$$

$$\begin{aligned} n_{eff,DFB}(T, I) &= n_{eff,DFB,0} \\ &+ \Delta T \frac{\partial n_{eff,DFB}(T, I)}{\partial T} \Big|_{I=I_{th}(T)} \\ &+ \Delta I(T) \frac{\partial n_{eff,DFB}(T, I)}{\partial I}, \quad (3) \end{aligned}$$

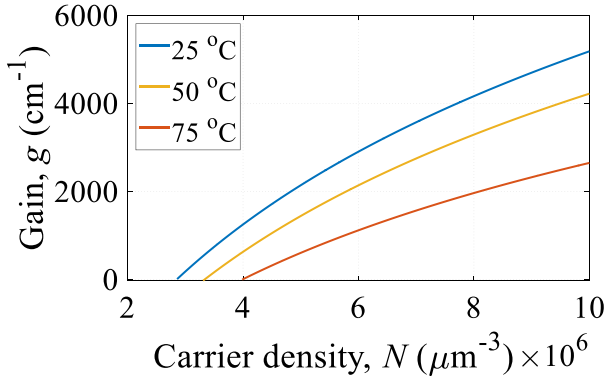
$$\begin{aligned} n_{eff,DFB,0} &\equiv n_{eff,DFB} \\ &(T = 25^\circ\text{C}, I = I_{th}(25^\circ\text{C})), \quad (4) \end{aligned}$$

$$\Delta T \equiv T - 25^\circ\text{C}, \quad (5)$$

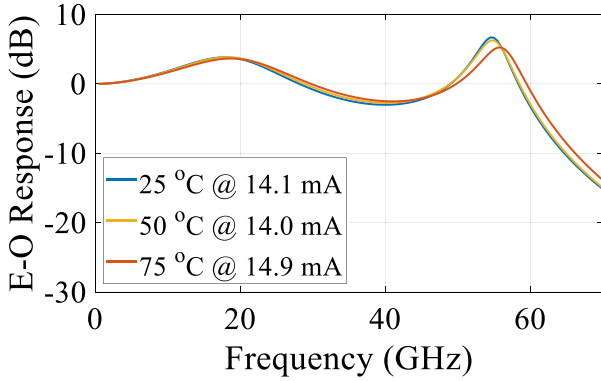
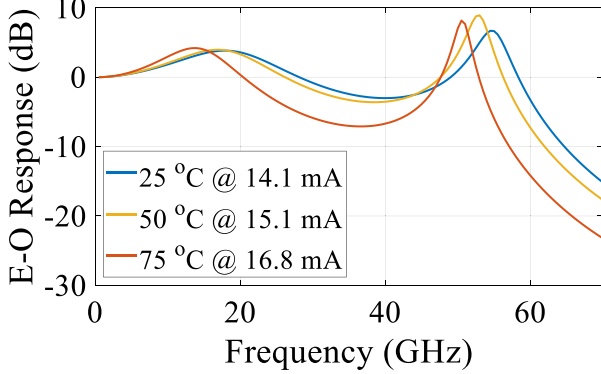
$$\Delta I(T) \equiv I - I_{th}(T). \quad (6)$$

The parameters $n_{eff,DBR,0}$, $n_{eff,DFB,0}$, $\frac{\partial n_{eff,DBR}}{\partial T}$, and $\frac{\partial n_{eff,DFB}}{\partial T} \Big|_{I=I_{th}(T)}$ were obtained by experimental spectra taken at different temperatures and subsequent estimations of the Bragg wavelengths of each section. The parameter $\frac{\partial n_{eff,DFB}}{\partial I}$ was fitted based on Fig. 8.

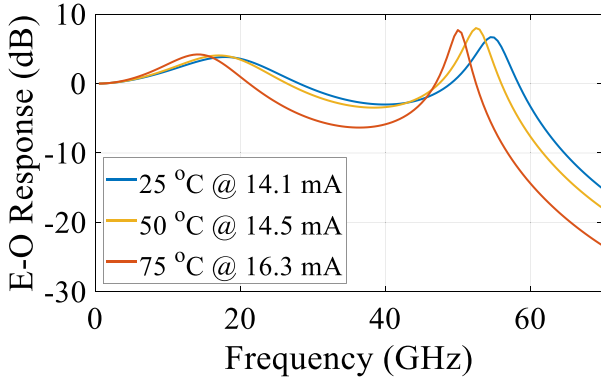
As it can be seen by Fig. 9(b) and Fig. 9(c), f_{PPR} is mainly defined by the temperature dependence of the gain and it has only a minor dependence on the temperature dependence of n_{eff} . The physical interpretation of this can be understood as follows: the reduction of the gain at higher temperatures requires that the main lasing mode “comes closer” in wavelength to the side-mode in order for the latter to receive sufficient power to appear in the E-O response. On the other hand, the temperature dependence of n_{eff} mainly defines the operating bias current for maximizing the bandwidth as discussed above. Finally, by combining the two effects, the simulated E-O response in Fig. 9(d) could demonstrate both the reduction of f_{PPR} at higher temperatures and the temperature dependence of the operating bias current for maximizing the modulation bandwidth. We believe that these results clarify the important relationship between f_{PPR} and temperature adequately for the first time.



(a) Gain fitting.

(b) E-O response: dependence on n_{eff} only.

(c) E-O response: dependence on gain only.

(d) E-O response: dependence on n_{eff} and gain.

V. CONCLUSION

We have demonstrated an energy-efficient two-channel membrane DML-array on SiO₂/Si with 60-GHz 3-dB bandwidth for optical interconnects, based on an optimized design for the PPR effect. 200 Gbps (2 \times 112-Gbps NRZ) with laser operating energy-per-bit cost of \sim 0.29 pJ/bit and the feasibility of 400 Gbps (2 \times 200-Gbps PAM-4) transmissions have been demonstrated based on this two-channel array. Finally, the temperature dependence of the PPR effect and its impact on the E-O response have been studied both experimentally and with numerical simulations for temperatures up to 75 °C.

REFERENCES

- [1] "Global cloud index: Forecast and methodology 2016-2021," Cisco, 2018. Accessed: Mar. 02, 2022. [Online]. Available: https://virtualization.network/Resources/Whitepapers/0b75cf2e-0c53-4891-918e-b542a5d364c5_white-paper-c11-738085.pdf
- [2] *IEEE Standard for Ethernet - Amendment 10: Media Access Control Parameters, Physical Layers, and Management, Parameters for 200 Gb/s and 400 Gb/s Operation*, IEEE Standard 802.3bs, 2017.
- [3] "2020 Ethernet roadmap," ethernet alliance, 2020. Accessed : Mar 02, 2022. [Online]. Available: <https://ethernetalliance.org/technology/2020-roadmap/>
- [4] "Optical connectivity options for 400 gbps and higher on-board optics," consortium for on-board optics (COBO), Nov. 2019. Accessed: Mar 02, 2022. [Online]. Available: <https://www.onboardoptics.org/race-to-800g-a-reality-check-micros-1>
- [5] Md. A. B. Siddik, A. Shehabi, and L. Marston, "The environmental footprint of data centers in the United States," *Environ. Res. Lett.*, vol. 16, no. 6, Jun. 2021, Art. no. 064017.
- [6] S. Matsuo and T. Kakitsuka, "Low-operating-energy directly modulated lasers for short-distance optical interconnects," *Adv. Opt. Photon.*, vol. 10, no. 3, pp. 567–643, Sep. 2018.
- [7] H. Nishi *et al.*, "Membrane distributed-reflector laser integrated with SiO_x-based spot-size converter on Si substrate," *Opt. Exp.*, vol. 24, no. 16, pp. 18346–18352, Aug. 2016.
- [8] N.-P. Diamantopoulos *et al.*, "47.5 GHz membrane-III-V-on-Si directly modulated laser for sub-pj/bit 100-Gbps transmission," *Photonics*, vol. 8, no. 2, p. 31, Jan. 2021.
- [9] T. Fujii, K. Takeda, H. Nishi, N.-P. Diamantopoulos, T. Sato, T. Kakitsuka, T. Tsuchizawa, and S. Matsuo, "Multiwavelength membrane laser array using selective area growth on directly bonded InP on SiO₂/Si," *Optica*, vol. 7, no. 7, pp. 838–846, Jul. 2020.
- [10] H. Nishi *et al.*, "Integration of eight-channel directly modulated membrane-laser array and SiN AWG multiplexer on Si," *J. Lightw. Technol.*, vol. 37, no. 2, pp. 266–273, Jan. 2019.
- [11] N.-P. Diamantopoulos *et al.*, "400-Gb/s DMT-SDM transmission based on membrane DML-array-on-silicon," *J. Lightw. Technol.*, vol. 37, no. 8, pp. 1805–1812, Apr. 2019.
- [12] G. Morthier, R. Schatz, and O. Kjebon, "Extended modulation bandwidth of DBR and external cavity lasers by utilizing a cavity resonance for equalization," *IEEE J. Quantum Electron.*, vol. 36, no. 12, pp. 1468–1475, Dec. 2000.
- [13] M. Radziunas *et al.*, "Improving the modulation bandwidth in semiconductor lasers by passive feedback," *IEEE J. Sel. Topics Quantum Electron.*, vol. 13, no. 1, pp. 136–142, Jan./Feb. 2007.
- [14] H. Dalir and F. Koyama, "Bandwidth enhancement of single-mode VCSEL with lateral optical feedback of slow light," *IEICE Electron. Exp.*, vol. 8, no. 13, pp. 1075–1081, Jul. 2011.
- [15] A. Abbasi *et al.*, "Direct and electroabsorption modulation of a III-V-on-Silicon DFB laser at 56 Gb/s," *IEEE J. Sel. Topics Quantum Electron.*, vol. 23, no. 6, Nov./Dec. 2017, Art. no. 1501307.
- [16] Y. Matsui *et al.*, "55 GHz bandwidth distributed reflector laser," *J. Lightw. Technol.*, vol. 35, no. 3, pp. 397–403, Feb. 2017.
- [17] Y. Matsui, R. Schatz, Di Che, F. Khan, M. Kwakernaak, and T. Sudo, "Low-chirp isolator-free 65-GHz-bandwidth directly modulated lasers," *Nature Photon.*, vol. 15, no. 1, pp. 59–63, Jan. 2021.

Fig. 9. Simulations on temperature dependence of E-O response.

- [18] S. Yamaoka *et al.*, "Directly modulated membrane lasers with 108 GHz bandwidth on a high-thermal-conductivity silicon carbide substrate," *Nature Photon.*, vol. 15, no. 1, pp. 28–35, Jan. 2021.
- [19] Di Che, Y. Matsui, Xi Chen, R. Schatz, and P. Iannone, "400-Gb/s direct modulation using a DFB+R laser," *Opt. Lett.*, vol. 45, no. 12, pp. 3337–3339, Jun. 2020.
- [20] N.-P. Diamantopoulos *et al.*, ">100-GHz bandwidth directly-modulated lasers and adaptive entropy loading for energy-efficient >300-Gbps/λ IM/DD systems," *J. Lightw. Technol.*, vol. 19, no. 3, pp. 771–778, Feb. 2021.
- [21] N.-P. Diamantopoulos, H. Nishi, W. Kobayashi, K. Takeda, T. Kakitsuka, and S. Matsuo, "On the complexity reduction of the second-order volterra nonlinear equalizer for IM/DD systems," *J. Lightw. Technol.*, vol. 37, no. 4, pp. 1214–1224, Feb. 2019.
- [22] N.-P. Diamantopoulos *et al.*, "2-channel 112-Gbps NRZ short-reach transmission based on 60-GHz-bandwidth directly-modulated membrane laser array on Si," in *Proc. ECOC*, Bordeaux, France, Sep. 2021, Art. no. Tu3D.3.
- [23] U. Feiste, "Optimization of modulation bandwidth in DBR lasers with detuned Bragg reflectors," *IEEE J. Quantum Electron.*, vol. 34, no. 12, pp. 2371–2379, Dec. 1998.
- [24] M. Radziunas and H.-J. Wünsche, "Multisection lasers: Longitudinal modes and their dynamics," in *Optoelectronic Devices*, J. Piprek, Ed., New York, NY, USA: Springer, 2005, pp. 121–150.
- [25] L. M. Zhang and F. R. Kschischang, "Staircase codes with 6% to 33% overhead," *J. Lightw. Technol.*, vol. 32, no. 10, pp. 1999–2002, May 2014.
- [26] B.-S. Kim, Y. Chung, and J.-S. Lee, "An efficient split-step time-domain dynamic modeling of DFB/DBR laser diodes," *IEEE J. Quantum Electron.*, vol. 36, no. 7, pp. 787–794, Jul. 2000.

Nikolaos-Pantaleimon Diamantopoulos (Member, IEEE) was born in Athens, Greece, in 1988. He received the B.Sc. degree from the University of Peloponnese, Tripoli, Greece, in 2009, the two M.Sc. degrees from Aston University, Birmingham, U.K., and Scuola Superiore Sant'Anna, Pisa, Italy, in 2012, under the joint-master's Erasmus Mundus Program, and the Ph.D. degree from Osaka University, Suita, Japan, in 2016. Between 2011 and 2016, he was involved in several EU-funded R&D projects with the Athens Information Technology Research Center, Greece. Since 2016, he has been with NTT Device Technology Labs, Japan. His research interests include integrated photonics, optical communications, signal processing, and semiconductor lasers. He is a Member of OPTICA.

Takuro Fujii (Member, IEEE) was born in Kyoto, Japan, in 1986. He received the B.E. and M.E. degrees in system design engineering from Keio University, Kanagawa, Japan, in 2010 and 2012, respectively. In 2012, he joined NTT Photonics Laboratories, Atsugi, Japan. His research interests include MOVPE growth of III–V semiconductors and the development of III–V semiconductor lasers on Si for photonic integrated circuits. He is a Member of IEICE and JSAP. He was the recipient of the Young Scientist Presentation Award from JSAP in 2014.

Suguru Yamaoka was born in Osaka, Japan, in 1993. He received the B.E., M.E., and Ph.D. degrees in applied physics from Osaka City University, Osaka, Japan, in 2015, 2017, and 2021, respectively. In 2017, he joined NTT Device Technology Labs, Atsugi, Japan. His research interests include high-speed and low-power-consumption directly modulated semiconductor lasers. He is a Member of IEICE and JSAP.

Hidetaka Nishi received the B.S. and M.S. degrees in mechanical science and engineering and the Ph.D. degree in electronics and applied physics from the Tokyo Institute of Technology, Tokyo, Japan, in 2005, 2007, and 2016, respectively. In 2007, he joined NTT Microsystem Integration Laboratories. Since then, he has been conducting research on integrated photonic and plasmonic devices. He is a Member of OPTICA and JSAP.

Koji Takeda (Senior Member, IEEE) received the B.S., M.S., and Ph.D. degrees in electronics engineering from the University of Tokyo, Tokyo, Japan, in 2005, 2007, and 2010, respectively. In 2010, he joined NTT Photonics Laboratories. His research interests include ultralow-power optical interconnects, InP photonic integrated circuits, and photonic crystal lasers. He is a Member of IEICE and JSAP. He was the recipient of the Best Student Paper Award from the IEEE Photonics Society in 2009 and the Outstanding Student Presentation Award from JSAP in 2010. From 2008 to 2010, he was the recipient of the Research Fellowship for Young Scientists from the Japan Society for the Promotion of Science.

Tai Tsuchizawa received the B.S. and M.S. degrees in physics from Sophia University, Tokyo, Japan, in 1984 and 1986, respectively, and the Ph.D. degree from the University of Tokyo, Tokyo, Japan, in 1990. He is currently a Distinguished Laboratory Specialist with NTT Device Technology Laboratories, Atsugi, Japan. In NTT's laboratories, he has been engaged in studies on ECR plasma and its application to etching process for microfabrication. His current research focuses on the fabrication technology for silicon-based optoelectronics devices. He is a Member of JSAP.

Toru Segawa (Member, IEEE) received the B.E. and M.E. degrees in electrical engineering and the Ph.D. degree in integrated design engineering from Keio University, Yokohama, Japan, in 1999, 2001, and 2012, respectively. In 2001, he joined NTT Photonics Laboratories, Atsugi, Japan, and has been engaged in research on high-speed tunable lasers and optical switches monolithically integrated on InP substrates. He is currently with the NTT Device Technology Laboratories, Atsugi, Japan. He is a Member of JSAP and IEICE.

Takaaki Kakitsuka (Member, IEEE) was born in Kumamoto, Japan, in 1971. He received the B.S. and M.S. degrees in physics and the Dr. Eng. degree from Kyushu University, Fukuoka, Japan, in 1994, 1996, and 2012, respectively. In 1996, he joined NTT Opto-Electronics Laboratories, NTT Corporation, Kanagawa, Japan. From 1996 to 2019, he was involved in research on semiconductor lasers and optical integrated devices with NTT Corporation. In 2019, he became an Associate Professor with the Graduate School of Information, Production and Systems, Waseda University, Fukuoka, Japan. His research interests include semiconductor lasers and their information communication system applications. He is a Member of IEICE, JSAP, and the Physical Society of Japan.

Shinji Matsuo (Fellow, IEEE) received the B.E. and M.E. degrees in electrical engineering from Hiroshima University, Hiroshima, Japan, in 1986 and 1988, respectively, and the Ph.D. degree in electronics and applied physics from the Tokyo Institute of Technology, Tokyo, Japan, in 2008. In 1988, he joined NTT Optoelectronics Laboratories, where he researched photonic functional devices using multiple quantum well pin modulators and VCSELs. In 1997, he researched optical networks using WDM technologies with NTT Network Innovation Laboratories. Since 2000, he has been researching high-speed tunable optical filters and lasers with NTT Photonics Laboratories, Atsugi, Japan, and NTT Device Technology Laboratories, Atsugi, Japan. He is a Senior Distinguished Researcher with NTT. He is a Member of JSAP, and IEICE, and a Fellow of OPTICA.